Strain engineering of photoinduced topological phases in two-dimensional ferromagnets

T. V. C. Antão [1] and N. M. R. Peres [2,3,4]

[1] *Laboratório de Instrumentação e Física Experimental de Partícuals (LIP), University of Minho, 4710-057 Braga, Portugal*
[2] *Centro de Física das Universidades do Minho e do Porto (CF-UM-UP) e Departamento de Física, Universidade do Minho, P-4710-057 Braga, Portugal*
[3] *International Iberian Nanotechnology Laboratory (INL), Av Mestre José Veiga, 4715-330 Braga, Portugal*
[4] *POLIMA—Center for Polariton-driven Light-Matter Interactions, University of Southern Denmark, Campusvej 55, DK-5230 Odense M, Denmark*

(Received 11 March 2023; revised 1 June 2023; accepted 1 June 2023; published 13 June 2023)

We argue that strain engineering is a powerful tool that may facilitate the experimental realization and control of topological phases in laser-driven two-dimensional (2D) ferromagnetic systems. To this extent, we show that by applying a circularly polarized laser field to a 2D honeycomb ferromagnet that is uniaxially strained in either the zigzag or armchair direction, it is possible to generate a synthetic Dzyaloshinskii-Moriya interaction tunable by the intensity of the applied electric field, as well as by the magnitude of applied strain. Such deformations enable transitions to phases with the opposite sign of the Chern number, or to trivial phases. These are basic results that could pave the way for the development of a new field of strain-engineered topological spintronics.

DOI: 10.1103/PhysRevB.107.235410

I. INTRODUCTION

With the experimental observation of magnetic order in two-dimensional (2D) materials in 2017 [1,2] and the simultaneous growth in interest in topological aspects of condensed-matter systems over the past decade, the ability to generate, study, and manipulate topological phases of magnetic materials has become a rapidly growing research direction. Systems such as magnon Chern insulators or other varieties of topological magnetic systems have been theoretically studied [3] and experimentally verified in the past few years [4,5]. The reason for this interest is that topology describes effects that stem from global properties of the band structure robust to small local perturbations, such as impurities, and they can have a profound effect on the material physical properties. Topological insulating phases are characterized, for instance, by the existence of chiral edge states with high mobility. Their robustness is desirable for a variety of applications such as spintronics, and for the ensuing technological implementations [6].

It is evident that for such applications, the ability to manipulate topological phases, whether by switching topological properties on or off, or by alternating between distinct topological phases, is a desirable goal.

Additionally, magnon-based approaches to spintronic technologies have also gained traction for a variety of reasons [7]: From their ability to propagate without generating electrical current and therefore reducing losses, to the possibility of making use of their internal degrees of freedom to implement logic gates [8,9], and to their large diffusion lengths in comparison to electrons [10–12], magnons have garnered attention as a convenient excitation for processing and transporting information. For this reason, magnon spintronics relies on the use of magnons as intermediate agents, being that information initially coded in the charge or spin of electrons can be converted to magnon currents, subsequently dispatched to and handled at potentially different devices, and finally converted back. In combination with the attractiveness of topology, the use of magnons renders the study of topological spin systems a worthwhile endeavor for the development of spintronic devices [13,14].

One possibility for engineering topology in spin systems relies on the fact that a 2D ferromagnet with a honeycomb lattice structure that hosts a strong intrinsic Dzyaloshinskii-Moriya interaction (DMI) [15,16] can have the magnitude of this interaction renormalized when irradiated by a circularly polarized laser field [17,18]. Indeed, it was predicted that CrI_3 hosts topological magnons at the **K** point of the hexagonal Brillouin zone, starting from a full electronic model [19].

A Heisenberg spin model (HSM) with a DMI provides a concrete realization of the Haldane model [20] for magnonic excitations. This model is known to host edge states, which are the hallmark of Chern insulator phases. Electronic Chern insulators, for instance, are able to conduct electrons along their edges and yet remain insulators in their bulk, and in a similar manner, magnonic insulator samples host gapless bands for spin excitations along their edges while remaining gapped in the bulk. This behavior results in a measurable thermal Hall response [21–25]. A field-dependent renormalization of the DMI can result in the possibility of the topological properties of spin systems being manipulated, such as the direction of edge-state conduction being reversed or entirely switched off, by changing the magnitude of the applied electric field. In addition, a DMI resulting entirely from the interaction of laser fields with spins [17] can also be generated. In this manner, if a material does not naturally host such an interaction, it can be synthesized by a laser beam, yielding a so-called Floquet magnon Chern insulator (FMCI). In case the material's intrinsic DMI is weak compared to such a synthetic term, the control of topological properties is limited: Increasing the intensity of the laser field can turn the interaction on or off, but it does not provide a way to reverse edge spin states or additional

desirable features. Besides, this limited tuning occurs only for very precise (and large) values of the intensity of the applied fields. Thus, if it were possible to induce this interaction in a fully tunable manner to a larger class of materials, one expects that new technological developments based on topological spintronics could arise. This paper addresses the manipulation of these topological states by proposing a method based on elastically deforming, i.e., straining, a 2D magnetic material. Strain can be applied in a variety of ways, including the deposition of a 2D material onto, and subsequent deformation of, an elastic substrate [26]. It has proven to be an extremely powerful tool in semiconductors, as well as in 2D materials such as graphene, where band-structure properties can be manipulated [27,28], and other electronic properties can be locally changed using patterned substrates. These patterns, such as bends or folds, wells, bubbles, and troughs, can induce mechanical strain on an overlaid monolayer of material, and they may be used to design all-graphene integrated circuits [29]. In Cr_2Te_3, strain-engineered magnetism has been observed [30], and when it comes to topology, strain in the Haldane model has also been theoretically considered in the past [31], where it has been shown to be able to induce topological phase transitions to a trivial state. The DMI can also be subject to changes due to strain [32], and this conjugation of factors is a good indicator that strain is a useful tool when considering topological properties of magnetic materials. We show here that this is indeed the case, as straining a 2D ferromagnet irradiated by a laser field can invert the sign of its topological invariant, as well as induce a transition from a topologically insulating phase to the trivial phase.

Our calculations, lying at the interface between strain engineering and Floquet engineering, may pave the way for a new class of strain-engineered topological spintronic (SETS) devices, based on local applications of strain to ferromagnetic 2D materials, as in this work we propose a mechanism for the realization of tunable photoinduced topology in a large class of 2D ferromagnetic materials based on strain. We draw phase diagrams based on the computation of the Floquet Chern number for a FMCI in the honeycomb lattice, as a function of tensile strain and the magnitude of an applied laser field which clearly exhibit strain-driven transitions. We consider two main cases: First, a next-nearest-neighbor (NNN) interaction is given by a DMI alone; and second, an extension of this model where one also considers an additional NNN Heisenberg coupling. We show that strain-induced topological phase transitions occur in both systems. However, due to the mapping between the latter model and an anisotropic Haldane model with the key property of tunable fluxes, phase transitions can occur for smaller electric field intensities and small amounts of strain. We argue that such a model could provide the breeding ground for new developments based on SETSs.

II. UNSTRAINED MODEL HAMILTONIAN AND LIMITATIONS

A. The Floquet magnon Chern insulator

We start by describing the basics of the magnetic model that serves as the basis for our proposal by considering the previously discussed FMCI in a honeycomb lattice of spin S atoms. The structure of the honeycomb lattice is given in panel

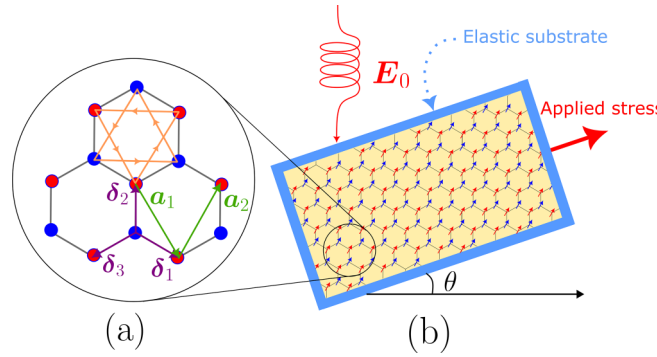

FIG. 1. (a) Honeycomb lattice structure: A (B) sublattice atoms are marked in blue (red). NN vectors $\boldsymbol{\delta}_i$ are displayed in purple, and NNN vectors $\boldsymbol{a}_i$ are displayed in green. Orange arrows in the topmost honeycomb shape showcase the flux factor of the Dzyaloshinskii-Moriya interaction. (b) Schematic for the setup for straining a ferromagnetic 2D material at an angle θ if stress is applied along the large blue arrow. An external electric circularly polarized electric field is applied with magnitude E_0 leading to the tunable topological properties described in the main text. Throughout the text, we will consider $\theta = 0$ corresponding to zigzag (ZZ) strain, and $\theta = \pi/2$ corresponding to armchair (AC) strain.

(a) of Fig. 1. It is a Bravais lattice with two atoms per unit cell and thus can be thought of as being composed of two distinct sublattices, which we label by A and B. An A-sublattice atom is connected to its nearest neighbors (NN) via the vectors

$$\boldsymbol{\delta}_1 = (\sqrt{3}/2, -1/2)a_0, \tag{1}$$

$$\boldsymbol{\delta}_2 = (0, 1)a_0, \tag{2}$$

$$\boldsymbol{\delta}_3 = (-\sqrt{3}/2, -1/2)a_0, \tag{3}$$

where a_0 is the interatomic distance, in a pristine, unstrained lattice. A 2D honeycomb ferromagnet can be described by a HSM Hamiltonian which depends on the spin vector operators $\boldsymbol{S}(\boldsymbol{r}_i) = (S^x(\boldsymbol{r}_i), S^y(\boldsymbol{r}_i), S^z(\boldsymbol{r}_i))$, acting at position $\boldsymbol{r}_i$, which can couple to spins at NN and NNN sites via in-plane exchange integrals $J_\perp$ and $J_{2,\perp}$, respectively, as well as their J_z and $J_{z,2}$ counterparts. The Hamiltonian reads explicitly

$$\begin{aligned} H = &\frac{1}{2}\sum_{\langle i,j\rangle} J_\perp S^+(\boldsymbol{r}_i)S^-(\boldsymbol{r}_j) + \text{H.c.} \\ &+ \frac{1}{2}\sum_{\langle\langle i,j\rangle\rangle} J_{2,\perp} S^+(\boldsymbol{r}_i)S^-(\boldsymbol{r}_j) + \text{H.c.} \\ &+ \sum_{\langle i,j\rangle} J_z S^z(\boldsymbol{r}_i)S^z(\boldsymbol{r}_j) + \sum_{\langle\langle i,j\rangle\rangle} J_{2,z} S^z(\boldsymbol{r}_i)S^z(\boldsymbol{r}_j), \end{aligned} \tag{4}$$

where $\langle\cdot,\cdot\rangle$ indicate a restriction of the summation to NN sites, and $\langle\langle\cdot,\cdot\rangle\rangle$ indicates a restriction to NNN sites. In addition, a representation in terms of the spin ladder operators $S^\pm = S^x \pm iS^y$ is used. This model hosts gapless Dirac magnon (quantized spin-wave) excitations whose bands showcase an ultrarelativistic dispersion near the $\boldsymbol{K}$ and $\boldsymbol{K}'$ points of the Brillouin zone.

An FMCI is built from a HSM quite subtly, as the fact that an electric field alone can couple to magnons, is, in

principle, not so obvious. The key effect that comes into play, which allows for the direct coupling of an electric field to neutral bosons which carry a magnetic moment, such as Dirac magnons, is the Aharonov-Casher (A-C) effect [33,34]. This is a dual effect to the more well known Aharonov-Bohm (A-B) effect [35], in which a charged particle in a region of space with zero magnetic field, but importantly nonzero magnetic vector potential, acquires a nontrivial topological phase. Both A-B and A-C effects can result in interference, and the A-C effect implies that a charge neutral particle with a magnetic moment moving in an electric field will also acquire such a phase, called the A-C phase. For a ferromagnet irradiated by a circularly polarized laser field $\boldsymbol{E}(t) = E_0(\tau\cos\omega t, \sin\omega t, 0)$, with handedness given by $\tau = \pm 1$, and with frequency ω, the A-C phase manifests itself as a time-dependent Peierls phase acquired by the Dirac magnons when hopping between different lattice sites.

The time dependence of the resulting Hamiltonian may appear initially cumbersome, as well as not particularly elucidating as to the underlying physical effects the Dirac magnons experience. For these reasons, a perturbative scheme has historically been considered for the analysis of such Hamiltonians, based on the analysis of periodically driven systems. This is the so-called Floquet theory. Using the Floquet theory framework, it is possible to perform a high-frequency expansion in inverse powers of ω [36] which provides an effective Hamiltonian up to $O(\omega^{-1})$ with clear qualitative and physical interpretation. The correction of lowest order $O(\omega^0)$ in high frequency provides an averaging of the Hamiltonian over a period of the driving laser, yielding a renormalization of the NN and NNN in-plane exchange integrals as $J_\perp \to J_\perp \mathcal{J}_0(\tau\alpha a_0)$, $J_{\perp,2} \to J_{\perp,2}\mathcal{J}_0(\tau\alpha\sqrt{3}a_0)$ [Eq. (5)], where $\alpha \equiv \mu_B E_0/\hbar c^2$, with μ_B the Bohr magneton. $\mathcal{J}_n(x)$ are the nth-order Bessel functions, and the constants $\hbar$ and c are the reduced Planck's constant and the speed of light in vacuum, respectively. The functional form of the renormalization of the NN in-plane hoppings is already interesting despite not providing topological properties by itself, as it depends on a Bessel function of order 0 for the case of the NN hoppings. This allows for tuning between Heisenberg-type couplings and Ising-type couplings, for instance, since all $J_\perp$ can be turned off. In the literature, one often defines the dimensionless parameter $\lambda = \alpha a_0$, however we make explicit here that the additional knob for this model, which is the key ingredient to the results showcased in this work, is the interatomic distance a_0.

In addition to this first-order correction, corresponding to the renormalization of $J_\perp$ and $J_{\perp,2}$, the second-order high-frequency correction can be seen to yield an additional term in the effective Hamiltonian, in the form of a spin-chirality [Eq. (6)]. The Hamiltonian will read $H_F = \hat{H}_F^{(1)} + \hat{H}_F^{(2)} + O(1/\omega^2)$, and the two first terms in the high-frequency expansion explicitly read

$$\hat{H}_F^{(1)} = -\sum_{\langle i,j\rangle} \frac{J_\perp \mathcal{J}_0(\tau\alpha a_0)}{2} S^+(\boldsymbol{r}_i)S^-(\boldsymbol{r}_j) + \text{H.c.} - \sum_{\langle i,j\rangle} J_z S^z(\boldsymbol{r}_i)S^z(\boldsymbol{r}_j) - \sum_{\langle\langle i,j\rangle\rangle} J_{2,z} S^z(\boldsymbol{r}_i)S^z(\boldsymbol{r}_j) - \sum_{\langle\langle i,j\rangle\rangle} \frac{J_{2,\perp}\mathcal{J}_0(\tau\alpha\sqrt{3}a_0)}{2} S^+(\boldsymbol{r}_i)S^-(\boldsymbol{r}_j) + \text{H.c.}, \tag{5}$$

$$\hat{H}_F^{(2)} = \sum_{\langle i,\langle j\rangle,k\rangle} \chi_{ijk}\boldsymbol{S}(\boldsymbol{r}_i)\cdot[\boldsymbol{S}(\boldsymbol{r}_j)\times\boldsymbol{S}(\boldsymbol{r}_k)]. \tag{6}$$

Here, the interlinked braces $\langle\cdot,\langle\cdot\rangle,\cdot\rangle$ indicate that the summation is performed over NNN atoms at positions i and k, which are connected by position j. In Eq. (6), the spin-chirality is given in magnitude by

$$\chi_{ijk} = \tau\sqrt{3}J^2\mathcal{J}_1(\tau\alpha\delta_{ji})\mathcal{J}_1(\tau\alpha\delta_{ik})\nu_{ik}^{A/B}/\omega, \tag{7}$$

where $\nu_{ik}^A = -\nu_{ik}^B = -\nu_{ki}^A$ is a fluxlike term, dependent on the orientation of the NNN bonds which connect sites i and k according to the orange arrows in Fig. 1, panel (a). Note that we have made clear the fact that the intensity of the spin-chirality depends on the successive hoppings between an intermediate site via the first-order Bessel functions. At this stage, all the distances $\delta_{ji} \equiv |\boldsymbol{\delta}_i|a_0 = a_0$ are the same, and they equal the interatomic distance. As such, we can write $\mathcal{J}_1(\tau\alpha\delta_{ji})\mathcal{J}_1(\tau\alpha\delta_{ik}) = \mathcal{J}_1^2(\tau\alpha a_0)$. This makes it so that $\text{sgn}(\chi) = \tau$ for any possible value of $\alpha \propto E_0$. Such a spin chirality term is known to originate frustration in the ground state of the ferromagnetic system, leading to the possibility of originating spin-liquid states [37], but considering $J_z > J_\perp$ the ferromagnetic ground state is stabilized.

For pursuing our discussion, a second quantization formalism for magnons can be employed using the Holstein-Primakoff (HP) bosonization. The (linearized) HP transformations map spin operators into bosonic creation and annihilation operators $a_i^\dagger/a_i$ $(b_i^\dagger/b_i)$ within the A (B) sublattices. Within linear spin-wave theory, the spin-chirality is indistinguishable from a DMI, and, indeed, when writing this term using HP operators, and retaining only terms up to second order in such operators, this equivalence becomes clear. A particularly useful way to write this Hamiltonian in momentum space can be achieved in terms of the Pauli matrices. If we consider the vector of creation operators $\Psi_{\boldsymbol{k}}^\dagger = (a_{\boldsymbol{k}}^\dagger, b_{\boldsymbol{k}}^\dagger)$, the effective Hamiltonian in momentum space can be written as

$$\mathcal{H}_F = \sum_{\boldsymbol{k}} \Psi_{\boldsymbol{k}}^\dagger[h_0(\boldsymbol{k})\mathbb{1} + \boldsymbol{h}(\boldsymbol{k})\cdot\boldsymbol{\sigma}]\Psi_{\boldsymbol{k}}, \tag{8}$$

where $\mathbb{1}$ is the 2×2 identity matrix, and we have defined a scalar $h_0(\boldsymbol{k})$ and a vector $\boldsymbol{h}(\boldsymbol{k}) = (h_x(\boldsymbol{k}), h_y(\boldsymbol{k}), h_z(\boldsymbol{k}))$ which is contracted with the vector of Pauli matrices $\boldsymbol{\sigma} = (\sigma_x, \sigma_y, \sigma_z)$. We will give an explicit form of the $\boldsymbol{h}(\boldsymbol{k})$ vector and the $h_0(\boldsymbol{k})$ scalar in a bit; however, let us first draw a useful comparison to the well-known Haldane model. For now, we note that this is a general way to write a 2×2 Hermitian operator, which is useful for our purposes, since the vector $\boldsymbol{h}(\boldsymbol{k})$ contains all the information necessary for the topological characterization of the system. For now, we note that it includes summations over the NN and NNN vectors, and thus it is expected that changing these vectors can have an effect on the spectrum as well as on the topological properties of this model. In the absence of a DMI, we have $h_z(\boldsymbol{k}) = 0$, the system is gapless, and hence it is in a trivial topological phase. Turning on the

DMI, the spectrum of Dirac magnons becomes gapped, and thus this interaction can be interpreted as providing Dirac magnons with a mass. This system then falls into the category of Chern insulators, for which the signature of topology is the Chern number or TKNN invariant [38], which takes nonzero integer values if the material is in a topological phase, and it is zero for a trivial phase. If the topology is photoinduced, one calls it the Floquet Chern number C_η^F, and in any case, it can be computed as an integral over the Berry curvature $\Omega_\eta^F(\boldsymbol{k}) = \frac{\eta}{2}\hat{\boldsymbol{h}}(\boldsymbol{k}) \cdot (\partial_{k_x}\hat{\boldsymbol{h}}(\boldsymbol{k}) \times \partial_{k_y}\hat{\boldsymbol{h}}(\boldsymbol{k}))$ in the full Brillouin zone, i.e.,

$$C_\eta^F = \frac{1}{2\pi}\int_{\mathrm{BZ}} d^2\boldsymbol{k}\Omega_\eta^F(\boldsymbol{k}). \tag{9}$$

In the expression for the Berry curvature and Floquet Chern number, $\hat{\boldsymbol{h}}(\boldsymbol{k}) = \boldsymbol{h}(\boldsymbol{k})/|\boldsymbol{h}(\boldsymbol{k})|$, and $\eta = \pm 1$ is the band index. The Berry curvature itself can also be computed from the eigenstates of the effective Hamiltonian using numerical approaches [39], but the analytical expression given above justifies the previous statement that the vector $\boldsymbol{h}(\boldsymbol{k})$ contains all relevant information necessary for the characterization of the material's topological properties. For the unstrained FMCI, we have the analytical result $C_\eta^F = \eta\tau\,\mathrm{sgn}(\chi)$, using the explicit form of $\boldsymbol{h}(\boldsymbol{k})$ given in Sec. II B. Our numerical calculations will employ Fukui's method [39] due to its efficiency, but they remain analytically verifiable.

Finally, we can make our introductory comments about the manipulation of topology being restricted in this model more precise. From the analytical results for C_η^F given a certain polarization of light τ, we have, so long as we set $J_{2,\perp} = 0$, the result $C_\eta^F = \eta\tau$, regardless of the intensity of the laser field, with the exception of very special points, at which $\mathcal{J}_1^2(\tau\alpha a_0) = 0$, at which $C_\eta^F = 0$. The guiding motivation for the following discussion is that this term stems from a more generic $\mathcal{J}_1(\tau\alpha\delta_{ji})\mathcal{J}_1(\tau\alpha\delta_{ik})$, and hence if interatomic distances could be changed, one could potentially switch the sign of the Chern number.

B. Mapping the FMCI to a bosonic Haldane model

In this section, we make explicit that the structure yielded by the FMCI corresponds to the bosonic Haldane model. This model is entirely analogous to its fermionic counterpart with the exception of being expressed at the cost of bosonic creation/annihilation operators in the A and B sublattices of a honeycomb structure. Bosons are created (annihilated) by $a_i^\dagger$ (a_i) in the A sublattice and by $b_i^\dagger$ (b_i) in the B sublattice. It reads

$$\begin{aligned} H = &\sum_i M(a_i^\dagger a_i - b_i^\dagger b_i) + \sum_{\langle i,j\rangle} t_{ij} a_i^\dagger b_i + \mathrm{H.c.} \\ &+ \sum_{\langle\langle i,j\rangle\rangle} t_{2,ij}(a_i^\dagger a_j + b_i^\dagger b_j) + \mathrm{H.c.} \\ &+ i\sum_{\langle\langle i,j\rangle\rangle} t'_{2,ij}(a_i^\dagger a_j - b_i^\dagger b_j) + \mathrm{H.c.} \end{aligned} \tag{10}$$

Here, M is called the Haldane mass, and both real ($t_{2,ij}$) and imaginary ($it'_{2,ij}$) NNN hoppings are present. One can bring the two NNN hopping terms together by writing $t_{2,ij} + it'_{2,ij} = t''_{2,ij}e^{i\nu_{ij}\phi_{ij}}$, where $\phi_{ij} = \arctan(t'_{2,ij}/t_{2,ij})$, and where $t''_{2,ij} = \sqrt{t_{2,ij}^2 + t_{2,ij}'^2}$. The factor $\nu_{ij} = \pm 1$ is then chosen according to the direction of the NNN hopping (see the orange arrows in Fig. 1). Thus, the Haldane model Hamiltonian can be written, up to an arbitrary energy shift, as

$$\begin{aligned} H = &\sum_i M(a_i^\dagger a_i - b_i^\dagger b_i) + \sum_{\langle i,j\rangle} t_{ij} a_i^\dagger b_i + \mathrm{H.c.} \\ &+ \sum_{\langle\langle i,j\rangle\rangle} t''_{2,ij} e^{i\nu_{ij}\phi_{ij}}(a_i^\dagger a_j - b_i^\dagger b_j). \end{aligned} \tag{11}$$

By writing the FMCI Hamiltonian, and specifically the second-order correction in terms of spin ladder operators, and subsequently using the HP transformations, the spin-chirality term becomes a purely imaginary NNN hopping. The identifications given in Table I can then be performed. Essentially, NN and NNN hoppings are mapped to their exchange integral counterparts, and the spin-chirality is mapped to an imaginary hopping, and a Haldane mass can exist, for instance, in ferrimagnetic systems (where it is not actually J_z, which is different for the sublattices, but rather the value of the spin S) [34].

Furthermore, the flux ϕ_{ij} becomes dependent on the intermediary site k between i and j, and it reads $\phi_{ijk} = \arctan(\frac{J_\perp^2\tau}{J_{2,\perp}\hbar\omega}\frac{\mathcal{J}_1(\alpha a_0)\mathcal{J}_1(\alpha a_0)}{\mathcal{J}_0(\alpha\sqrt{3}a_0)})$, and with this mapping underway, a momentum space representation can be readily constructed by considering $\boldsymbol{h}(\boldsymbol{k})$ and $h_0(\boldsymbol{k})$ given by

$$h_0(\boldsymbol{k}) = -\sum_j t''_{2,j}\cos\phi_j\cos(\boldsymbol{k}\cdot\boldsymbol{a}_j), \tag{12}$$

$$h_x(\boldsymbol{k}) = -\sum_j t_j\cos(\boldsymbol{k}\cdot\boldsymbol{\delta}_j), \tag{13}$$

$$h_y(\boldsymbol{k}) = \sum_j t_j\sin(\boldsymbol{k}\cdot\boldsymbol{\delta}_j), \tag{14}$$

$$h_z(\boldsymbol{k}) = M - 2\sum_j t''_{2,j}\sin\phi_j\sin(\boldsymbol{k}\cdot\boldsymbol{a}_j). \tag{15}$$

TABLE I. Identifications between the Haldane model and the Floquet magnon Chern insulator for the case in which no strain is present.

Haldane	FMCI
t	$3J_\perp S\mathcal{J}_0(\alpha\delta_{ij})$
t_2	$3J_{2,\perp}S\mathcal{J}_0(\alpha a_{ij})$
t_2'	$6J_\perp^2S^2\tau\mathcal{J}_1(\alpha a_0)\mathcal{J}_1(\alpha a_0)/\hbar\omega$
M	$(J_{z,A} - J_{z,B})S/2$

The inclusion of strain must now account for several physical phenomena, i.e., it must describe changes in bond lengths and subsequent anisotropic variations in hopping and exchange interactions. In the following section, a simple model that describes such variations is introduced.

III. EFFECTS OF STRAIN ON TOPOLOGICAL PROPERTIES

A. FMCI with NN hoppings

As we have previously described, for a magnetic material with a strong intrinsic DMI, the sgn(χ) can be manipulated by changing the intensity of the laser field, due to the first-order correction of the high-frequency approximation, which reads $\chi \to \mathcal{J}_0(\alpha a_0)\chi$. For systems in which the DMI is fully synthetic and results only from second-order Floquet theory, this does not appear possible due to the dependence in $\mathcal{J}_1^2(\tau\alpha a_0) > 0$. Guided by the fact that a sign change can be achieved by making the system anisotropic and transforming $\mathcal{J}_1^2(\tau\alpha a_0) \to \mathcal{J}_1(\tau\alpha\delta_{ji})\mathcal{J}_1(\tau\alpha\delta_{ik})$, we now explore the uniaxial straining of an FMCI, and we show that even small amounts of strain can provide a pathway for topological manipulations of the model. Note that studies on the exchange parameters in CrI_3 as a function of strain have been considered and theoretically analyzed in the past, considering strain values up to 10% [40].

In the honeycomb lattice, the strain tensor is described by two parameters alone, namely the tensile strain ε and the Poisson ratio ν [41]. When inducing stress onto the 2D magnetic material, the tensile strain ε is proportional to this stress, and therefore we can treat ε as the tunable parameter in our system. It measures the amount of deformation in the direction of the applied stress, while the Poisson ratio measures the deformation of the lattice in the transverse direction. A positive Poisson ratio $\nu > 0$ indicates that when a material is stretched in a particular direction, it compresses in the transverse direction, and vice versa. As such, the lattice vectors acquire a functional dependence on the parameters ε and ν as strain applied in a particular direction. The deformed vectors read $\boldsymbol{\delta}_i(\varepsilon, \nu, \theta) = (1 + \bar{\bar{\varepsilon}})\boldsymbol{\delta}_i^{(0)}$, where the strain tensor is

$$\bar{\bar{\varepsilon}} = \begin{bmatrix} \varepsilon\cos^2\theta - \nu\sin^2\theta & (1+\nu)\cos\theta\sin\theta \\ (1+\nu)\cos\theta\sin\theta & \sin^2\theta - \nu\cos^2\theta \end{bmatrix}. \tag{16}$$

In the simplest tight-binding approach, strain can be included in a given Hamiltonian via modifying hopping amplitudes anisotropically. In previous works in the honeycomb lattice, it is considered that electronic hoppings are exponentially suppressed when the bond length is increased [42]. This is the simplest possible model, which can be intuited phenomenologically from the overlap of atomic orbitals. One has

$$(\mathrm{NN}) : t_{ij} = t^{(0)} e^{-\beta\left(\delta_{ij}(\varepsilon,\nu,\theta)-1\right)}, \tag{17}$$

$$(\mathrm{NNN}) : t_{2,ij} = t_2^{(0)} e^{-\beta\left(a_{ij}(\varepsilon,\nu,\theta)-\sqrt{3}\right)}, \tag{18}$$

where β is a phenomenological parameter of the order of unity. Since we expect that the strength of the exchange interaction is $J \propto t^2/U$ for U representing the strength of on-site Coulomb repulsion in some underlying electronic model, we consider that a similar exponential decay occurs for J with the rate of 2β. We find that the inclusion of such a phenomenological correction in a standard Haldane model is enough to produce topological phase transitions, when a system is strained in the zigzag direction with values of, for instance, $\varepsilon \sim 15\%$ for a Haldane flux of $\phi = 4\pi/5$, due to a fusion of the magnonic Dirac points. This is presented in Fig. 2. For a standard DMI system, if $J_{2,z/\perp} = 0$, i.e., a Haldane flux is present corresponding to $\phi = \pi/2$, the critical strain necessary for a topological phase transition can be much higher, making it unfeasible for realistic applications. On the other hand, rich phase diagrams emerging from uniaxially straining a FMCI can appear. This is due to the intricate dependence of NN and NNN hoppings on Bessel functions, as presented in Table II. We focus first on the simplest case, with $J_{2,z} = J_{2,\perp} = 0$, but we will show later that the inclusion of these terms yields several advantages.

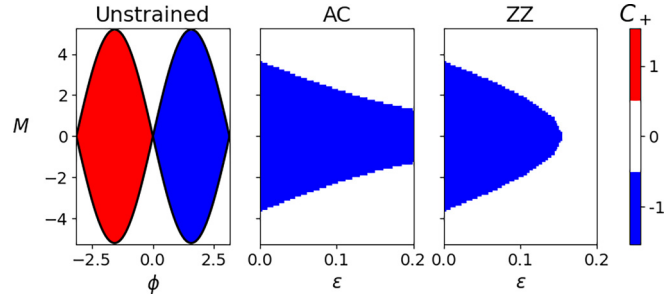

FIG. 2. The leftmost panel showcases the phase diagram for a bosonic Haldane model as a function of the Haldane mass M and the phase ϕ. Black lines in this panel indicate $M = \pm 3\sqrt{3}\sin\phi$, which are the analytical results for the phase transition lines in this model. The right panels showcase phase diagrams for the strained bosonic Haldane model in the zigzag (ZZ) and armchair (AC) directions. We pick $\beta = 6.74$, $\nu = 0.165$, and a phase of $\phi = 4\pi/5$, such that for strain applied in the ZZ direction, for any value of M and a strain above ∼15%, the model is in a trivial phase. Generically, for strain in the AC direction, no phase transitions are observed for $M = 0$.

The functional dependence on Bessel functions can result in the closing of the gap of the system well below strain values of 15%, and can break the symmetry of the lattice in such a way that the system becomes topologically trivial, or even switch the relative sign of NN and DMI. Indeed, this NN sign-switch plays a more relevant role at a lower value of the intensity of the electric field for any reasonable value of strain. Thus, from an experimental point of view, it may be more easily accessed. Figure 3 shows that if stress is applied in the zigzag as well as armchair directions of the honeycomb lattice, there exist several points, near the zero of $\mathcal{J}_0(\alpha|\delta_1(\varepsilon,\nu,\theta)|a_0) = \mathcal{J}_0(\alpha|\delta_3(\varepsilon,\nu,\theta)|a_0)$, at which a transition between a Floquet Chern number $C_-^F = -1$ to $C_-^F = 1$ can occur, even for very small values of strain. For strain applied in the armchair (AC) direction, a large region of Chern number $C_-^F = +1$ occurs for strain above 12.5% and αa_0 above the first zero of $\mathcal{J}_0$, whereas for strain applied in

TABLE II. Identifications between the Haldane model and strained Floquet magnon Chern insulator.

Haldane	Strained FMCI
t	$3J_\perp S\mathcal{J}_0(\alpha\delta_{ij})e^{-2\beta(\delta_{ij}-1)}$
t_2	$3J_{2,\perp}S\mathcal{J}_0(\alpha a_{ij})e^{-2\beta(a_{ij}-\sqrt{3})}$
t_2'	$6J_\perp^2 S^2\tau\mathcal{J}_1(\alpha\delta_{ik})\mathcal{J}_1(\alpha\delta_{kj})e^{-2\beta(\delta_{ik}+\delta_{kj}-2)}/\hbar\omega$
M	$(J_{z,A} - J_{z,B})S/2$

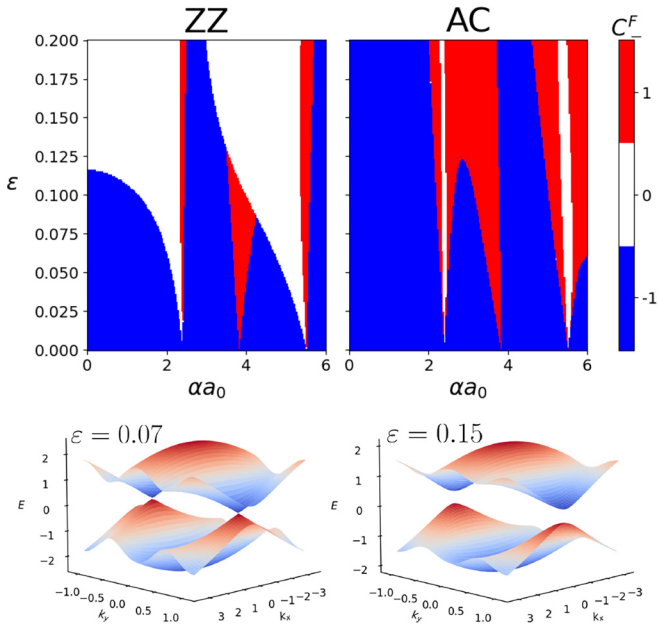

FIG. 3. Upper panels: Phase diagrams showcasing the Chern number as a function of the electric field through αa_0 as well as the strain magnitude ε in the ZZ and AC directions for a FMCI with $J_2 = 0$ and $\hbar\omega = 50J$. Left panel: Strain in the ZZ direction: A series of dips is observable for which at certain values of electric field, small amounts of strain are necessary to induce a topological phase transition. The first white dip corresponds to a situation where $\mathcal{J}_0(\alpha|\delta_1|a_0)$ and $\mathcal{J}_0(\alpha|\delta_3|a_0)$ go to zero. The subsequent transitions in each dip occur either because of this or due to changes in the DMI sign due to $\mathcal{J}_1$. Right panel: Strain in the AC direction: A similar situation occurs, with the first dip being related to the position of the zero of the NN exchange integrals, and the second dips occur due to the DMI sign change. Lower Panels: Band structure of the FMCI for a small value of electric field $\alpha a_0 = 0.01$ and strain along the ZZ direction. The left and right panels provide an example of the band structure below and above the critical strain, respectively. The transition from topological to trivial phases occurs due to the merging of the Dirac cones at the edge of the Brillouin zone. The topological gap in the left panel's band structure is practically invisible due to the small magnitude of electric field, which illustrates a difficulty inherent to the implementation of realizing photoinduced topological magnons with NN interactions alone.

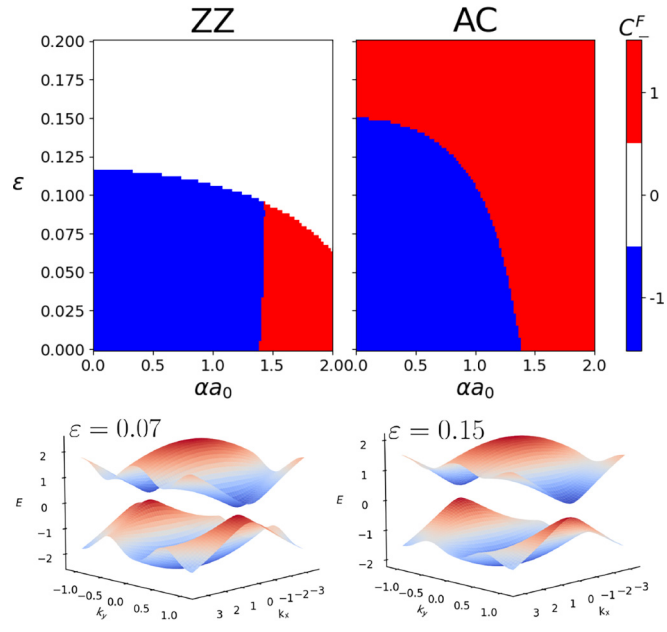

FIG. 4. Upper panels: Phase diagrams showcasing the Chern number as a function of the electric field through αa_0 as well as the strain magnitude ε in the zigzag (left panel) and armchair (right panel) directions, with $J_2 = 0.1J$ and $\hbar\omega = 50J$. For strain in the armchair direction, there exist critical strain values for a field arbitrarily close to zero, as well as critical field values for arbitrarily small strain near $\alpha a_0 \approx 1.38$, for which topological transitions can occur between phases with inverse Chern numbers. Lower panels: Band structure for a small value of electric field $\alpha a_0 = 0.01$ and strain in the ZZ direction. The left and right panels provide an example of the band structure below and above the critical strain, respectively. The presence of a NNN exchange integral $J_2 > 0$ clearly increases the gap (see Fig. 2) and further stabilizes the topological phase, reducing the necessary values of electric fields for the realization of photoinduced topology.

the ZZ direction, transitions to a trivial phase can occur for a much smaller field intensity.

The generic behavior of the transitions is that several dips in critical strain occur within the phase diagram, close to zeros of the Bessel functions $\mathcal{J}_0$ and $\mathcal{J}_1$. As described in the section on realistic parameter values, $\alpha a_0 = 2.3$, which corresponds to the location of the first dip for which transitions occur for low values of strain, is still quite a large field intensity. This leads to the question of whether there exists any mechanism that can lower this critical value further.

B. FMCI with NNN hoppings

We now show that by turning on the NNN exchange integral $J_2 > 0$, which is renormalized by the laser field, the mapping to the Haldane model must also include a flux $\phi_{ijk} = \arctan(\chi_{ijk}/J_{2,ik})$, and since both of the quantities χ_{ijk} and $J_{2,ik}$ depend on αa_i in distinct manners. This phase becomes tunable with the electric field intensity, leading to another mechanism for tuning the topological phase. In this case, the phase diagram acquires two interesting features showcased in Fig. 4, especially evident for strain applied in the AC direction. A critical value of electric field exists that provides a transition for vanishing values of strain for a much lower value of electric field $\alpha a_0 \approx 1.38$. The value for the critical electric field is also decreased until it vanishes, at a strain of about 15%. Tuning the strain with high precision near this value can allow for an inversion of the sign of the Floquet Chern number for an arbitrarily small electric field. In the ZZ direction, a similar situation occurs for a topological to trivial transition, near 11% strain, and this value can be reduced to about 9.5% strain while remaining in the $C^F_- = -1$ phase by increasing α. Furthermore, as is clear from the inspection and comparison of the band structure of the FMCI in a nontrivial phase of Figs. 3 and 4, the presence of a J_2 term leads to a stabilization of the topological phase. Even for small electric fields, this term ensures a much larger gap will appear, thus rendering the FMCI far more amenable to experimental realizations. We consider these to be the most important results of this work,

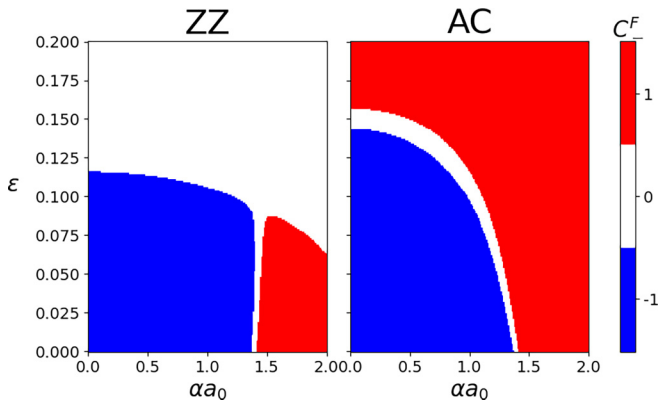

FIG. 5. Phase diagrams for the Floquet magnon Chern insulator with a finite mass $M = 3.3 \times 10^{-3} JS$. For these images we pick $\beta = 3.37$ and $\nu = 0.165$.

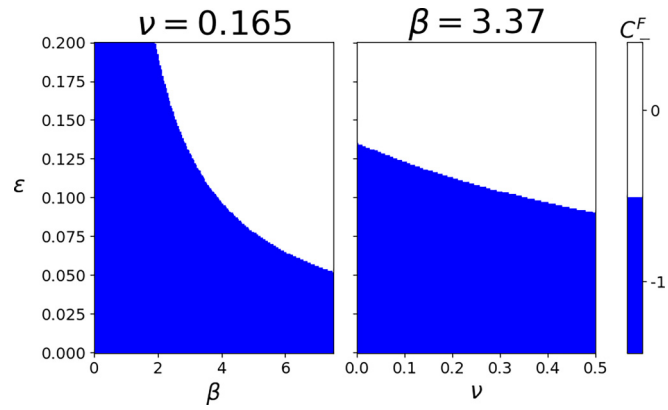

FIG. 6. Phase diagrams for the Floquet magnon Chern insulator with a small applied electric field $\alpha a_0 = 0.01$ and varying strain in the ZZ direction as well as parameters β (left) and ν (right). When one such parameter is varied, the other is kept constant at the values considered in the remainder of the text. Increasing either β or ν results in the lowering of the critical strain, which induces a topological phase transition.

as small values of strain can be achieved by overlaying a 2D magnetic material in a patterned substrate, and thus precise control of topological phases can be obtained in integrated devices. Another aspect that is also worth mentioning is that in the limit where $M \to 0$, the transitions between phases with opposite Chern number occur directly, as can be seen in Fig. 4 of the main text. On the other hand, for $M > 0$, finite regions of trivial phases crop up in between those characterized by Floquet Chern number $C_-^F = -1$ and $+1$, as seen in Fig. 5. This results in an intermediate phase with $C_-^F = 0$, which may be useful in an experimental context, as it provides a clear barrier between distinct topological phases.

IV. PARAMETER VALUES AND REALISTIC REALIZATION

We can now review and justify the choice of parameters used for our calculations, since some are still undetermined experimentally at the present time. Parameters such as the Poisson ratio ν for monolayer ferromagnetic materials, for instance, have not yet been subject to thorough experimental analysis, and hence for a rough estimate of the effects of the strain we have used $\nu = 0.165$ corresponding to the case of graphene, the most well-known 2D material with a honeycomb structure [28]. We also pick $\beta = 3.37$, corresponding to the value obtained experimentally for graphene [43]. The electric field at which the first transition occurs for small strain lies around $\alpha a_0 \approx 2.3$, but it is lowered for increased values of strain in the AC direction in the case of $J_2 = 0$. Using the distance between magnetic atoms in CrI_3 as a rough estimate, a critical electric field of the order of $E_0 \approx 1 \times 10^{13}$ V/cm is necessary to induce a transition. Lasers of up to 10^{23} W/cm^2 have been reported [44], which allow for laser fields of up to roughly $E_0 \approx 9 \times 10^{12}$ V/cm. Although this value is of the order of magnitude of the field necessary to induce topological phase transitions in the system, the authors recognize that it still is quite a high value of electric field, which may result in damage to the material or otherwise undesirable out-of-equilibrium phenomena to take place. This renders the topological phase transitions in a $J_2 = 0$ model likely out of reach. However, as our calculations show, for $J_2 > 0$, the critical electric fields are much smaller, and the topological gap is stabilized, facilitating an experimental implementation in essentially every regard. For increasing values of strain in the AC direction up to a critical value of 15%, a transition occurs for vanishing field intensity (see Fig. 4). In the ZZ direction, a trivial phase can be reached for values of up to 11% strain. Furthermore, we use $\hbar\omega = 50J$, which leads to a frequency of $\omega/2\pi \approx 1.2 \times 10^{13}$ Hz, lying in the 10s of THz, achievable using ultrafast terahertz spectroscopy [17]. It should also be noted that, for 2D ferromagnetic materials, our choice of parameters is a conservative estimate. Since graphene is known to have very strong carbon-carbon bonds, it is expected that realistic values of β may be much larger for other relevant materials, compatible with a quicker decay of electronic bond strengths. This actually reduces critical strain values. For instance, if β is doubled, strain in the ZZ direction can cause a topological phase transition at magnitudes as low as 5%. On the other hand, it may be the case that ν is actually smaller, and this would, in turn, result in an increased critical strain magnitude. This points to a necessity of further exploring elastic properties of 2D magnetic materials. The variation of the critical strain magnitude in the ZZ direction with both β and ν is given in Fig. 6. It is also worth noting that increasing the strength of J_2 does not alter the phase diagrams presented in any way, although it does increase the magnitude of the topological gap. Hence, if a material actually exhibits a greater value of J_2, this can ameliorate the conditions for a physical implementation of SETS.

Finally, and in order to discuss an alternative system in which our ideas could be tested, it is worth mentioning that the coupling between electrons and electric fields is much stronger. A number of papers have proposed the realization and study of photoinduced spin-liquid ground states starting from a Fermi-Hubbard model, realizable in cold atom lattices or some van der Waals materials [45–48]. Such a system would be described by a Hamiltonian of the form

$$H = -t \sum_{\langle i,j \rangle} e^{i\theta_{ij}(t)} c_{i\sigma}^\dagger c_{j\sigma} + U \sum_i \hat{n}_{i\uparrow} \hat{n}_{i\downarrow}, \qquad (19)$$

where the time-dependent Peierls phases $\theta_{ij}(t)$ now couple to electronic creation and annihilation operators $c^{\dagger}_{i\sigma}/c_{i\sigma}$. Here U is the Hubbard on-site Coulomb interaction which is proportional to the number of electrons $\hat{n}_{i\sigma} = c^{\dagger}_{i\sigma}c_{i\sigma}$ with opposite spins $\sigma = \uparrow, \downarrow$ occupying any given lattice site. A similar approach to the high-frequency approximation can be considered, in the spirit of the Schrieffer-Wolff transformation, where U is treated at the same level as the frequency $\hbar\omega$. The resulting effective Hamiltonian also exhibits a spin chirality with similar dependencies on Bessel functions [45]. Thus, an effective Heisenberg model with topological properties can be obtained, and the manipulation of its topological properties would proceed in exactly the same manner as we have described throughout this work. The advantage in our model is that the direct coupling to the spin system provides a much simpler and essentially physically equivalent treatment of the topological spin system, with the main difference being that directly coupling to electrons yields a number of advantages that may prove relevant for physical implementations: First, the coupling factors for magnons α_m and for electrons α_e are related by $\alpha_m/\alpha_e = 10^{-5}$ for a frequency of $\hbar\omega = 1$ eV, enabling the ability to obtain similar phenomenology for electric fields 10^5 times smaller. Additionally, the driving frequency can be chosen to be subgap, i.e., $\hbar\omega < U$, as well as off-resonant with U/n, where n is an integer. This means the electronic bands will remain at half-filling when driven by the laser field, thus avoiding material damage. A HSM plus a spin-chirality term can thus remain a valid description of the model under driving. Finally, electric fields of $E_0 \approx 1 \times 10^7$ V/cm can be utilized, which are well within reach of experiments, and allow for $\alpha a_0 > 1$, reaching most of the relevant parameter space for our proposal. It is our expectation that by manipulating the intensity of laser traps, deformed lattices could be realized in this setting, providing a possible mechanism to test our ideas in a more controlled environment.

V. CONCLUSIONS AND OUTLOOK

In this work, we have analyzed a Floquet magnon Chern insulator (FMCI) consisting of a honeycomb 2D ferromagnet upon which a circularly polarized laser beam is shone. The FMCI, by itself, can host topological bands with a quantized Floquet Chern number synthesized by the laser field. This synthetic topology is not easily tuned, and hence we propose a strain-engineering approach to increase the ability to manipulate the topological invariant using the laser field. We argue that this ability can lead to the development of new spintronics-based technologies. Having studied the case of a nearest-neighbor as well as next-nearest-neighbor exchange interaction within the original ferromagnet, we show that in the latter case, the topological invariant can become very sensitive to small amounts of strain for certain values of electric field intensities, and vice versa. Using our parameters, strain on the order of 10% can be used to make a FMCI undergo topological phase transitions for very small electric field intensities, or equivalently, using electric fields on the order of $E_0 \approx 1 \times 10^{12}$ V/cm, one can use small amounts of strain to generate topological phase transitions, which enables the possibility of using, for instance, patterned substrates for locally manipulating topological invariants, and generating edge spin current circuits.

Furthermore, existing devices based on topological magnons, such as magnon diodes, beam-splitters, or even Mach-Zender-type interferometers [14], could be realized by local variations in strain alone, not relying on changes in magnetization, or the creation of holes in the material, but rather on SETS.

We finally argue that systems based on cold-atom traps can function as a testing ground for these ideas, since coupling of electric fields to underlying electronic models of magnetism is much stronger than to spin systems directly due to the nature of the Aharonov-Casher effect. Within these models, it is nonetheless possible to generate topological magnetic terms such as a spin-chirality, and strain could be implemented in a simple manner by deforming the cold atom lattice.

ACKNOWLEDGMENTS

The authors thank António Costa and Joaquin Férnandez-Róssier for comments on this manuscript. T.V.C.A. acknowledges support by the Portuguese Foundation for Science and Technology (FCT) in the framework of the Project No. CERN/FIS-COM/0004/2021 and the hospitality of LIP where this work was conducted. N.M.R.P. acknowledges support by the Portuguese Foundation for Science and Technology (FCT) in the framework of the Strategic Funding UIDB/04650/2020, COMPETE 2020, PORTUGAL 2020, FEDER, and through projects PTDC/FIS-MAC/2045/2021, EXPL/FIS-MAC/0953/2021, and from the European Commission through the project Graphene Driven Revolutions in ICT and Beyond (Ref. No. 881603, CORE 3). Additionally, N.M.R.P. acknowledges support from the Independent Research Fund Denmark (Grant No. 2032-00045B) and the Danish National Research Foundation (Project No. DNRF165).

[1] C. Gong, L. Li, Z. Li, H. Ji, A. Stern, Y. Xia, T. Cao, W. Bao, C. Wang, Y. Wang, Z. Q. Qiu, R. J. Cava, S. G. Louie, J. Xia, and X. Zhang, Nature (London) **546**, 265 (2017).

[2] B. Huang, G. Clark, E. Navarro-Moratalla, D. R. Klein, R. Cheng, K. L. Seyler, D. Zhong, E. Schmidgall, M. A. McGuire, D. H. Cobden, W. Yao, D. Xiao, P. Jarillo-Herrero, and X. Xu, Nature (London) **546**, 270 (2017).

[3] L. Zhang, J. Ren, J.-S. Wang, and B. Li, Phys. Rev. B **87**, 144101 (2013).

[4] Z. Cai, S. Bao, Z.-L. Gu, Y.-P. Gao, Z. Ma, Y. Shangguan, W. Si, Z.-Y. Dong, W. Wang, Y. Wu, D. Lin, J. Wang, K. Ran, S. Li, D. Adroja, X. Xi, S.-L. Yu, X. Wu, J.-X. Li, and J. Wen, Phys. Rev. B **104**, L020402 (2021).

[5] R. Chisnell, J. S. Helton, D. E. Freedman, D. K. Singh, R. I. Bewley, D. G. Nocera, and Y. S. Lee, Phys. Rev. Lett. **115**, 147201 (2015).

[6] Q. L. He, T. L. Hughes, N. P. Armitage, Y. Tokura, and K. L. Wang, Nat. Mater. **21**, 15 (2022).

[7] Z. Li, Y. Cao, and P. Yan, *Topology in Collective Magnetization Dynamics* (IOP, Bristol, UK, 2023).

[8] T. Schneider, A. A. Serga, B. Leven, B. Hillebrands, R. L. Stamps, and M. P. Kostylev, Appl. Phys. Lett. **92**, 022505 (2008).

[9] M. Balynskiy, H. Chiang, D. Gutierrez, A. Kozhevnikov, Y. Filimonov, and A. Khitun, J. Appl. Phys. **123**, 144501 (2018).

[10] L. Cornelissen, J. Liu, R. Duine, J. Ben Youssef, and B. van Wees, Nat. Phys. **11**, 1022 (2015).

[11] P. Pirro, T. Brächer, A. V. Chumak, B. Lägel, C. Dubs, O. Surzhenko, P. Görnert, B. Leven, and B. Hillebrands, Appl. Phys. Lett. **104**, 012402 (2014).

[12] C. Liu, J. Chen, T. Liu, F. Heimbach, H. Yu, Y. Xiao, J. Hu, M. Liu, H. Chang, T. Stueckler, S. Tu, Y. Zhang, Y. Zhang, P. Gao, Z. Liao, D. Yu, K. Xia, N. Lei, W. Zhao, and M. Wu, Nat. Commun. **9**, 738 (2018).

[13] X. S. Wang, Y. Su, and X. R. Wang, Phys. Rev. B **95**, 014435 (2017).

[14] X. S. Wang, H. W. Zhang, and X. R. Wang, Phys. Rev. Appl. **9**, 024029 (2018).

[15] I. Dzyaloshinsky, J. Phys. Chem. Solids **4**, 241 (1958).

[16] T. Moriya, Phys. Rev. **120**, 91 (1960).

[17] S. A. Owerre, J. Phys. Commun. **1**, 021002 (2017).

[18] S. A. Owerre, J. Phys. Commun. **2**, 109501 (2018).

[19] A. T. Costa, D. L. R. Santos, N. M. R. Peres, and J. Fernández-Rossier, 2D Mater. **7**, 045031 (2020).

[20] F. D. M. Haldane, Phys. Rev. Lett. **61**, 2015 (1988).

[21] H. Katsura, N. Nagaosa, and P. A. Lee, Phys. Rev. Lett. **104**, 066403 (2010).

[22] Y. Onose, T. Ideue, H. Katsura, Y. Shiomi, N. Nagaosa, and Y. Tokura, Science **329**, 297 (2010).

[23] R. Matsumoto and S. Murakami, Phys. Rev. Lett. **106**, 197202 (2011).

[24] R. Matsumoto, R. Shindou, and S. Murakami, Phys. Rev. B **89**, 054420 (2014).

[25] J. H. Han and H. Lee, J. Phys. Soc. Jpn. **86**, 011007 (2017).

[26] Z. Peng, X. Chen, Y. Fan, D. J. Srolovitz, and D. Lei, Light Sci. Appl. **9**, 190 (2020).

[27] T. Low, F. Guinea, and M. I. Katsnelson, Phys. Rev. B **83**, 195436 (2011).

[28] V. M. Pereira, A. H. Castro Neto, and N. M. R. Peres, Phys. Rev. B **80**, 045401 (2009).

[29] V. M. Pereira and A. H. Castro Neto, Phys. Rev. Lett. **103**, 046801 (2009).

[30] J. Zhong, M. Wang, T. Liu, Y. Zhao, X. Xu, S. Zhou, J. Han, L. Gan, and T. Zhai, Nano Res. **15**, 1254 (2022).

[31] M. Mannaï and S. Haddad, J. Phys.: Condens. Matter **32**, 225501 (2020).

[32] O. G. Udalov and I. S. Beloborodov, Phys. Rev. B **102**, 134422 (2020).

[33] Y. Aharonov and A. Casher, Phys. Rev. Lett. **53**, 319 (1984).

[34] A. S. T. Pires, *Theoretical Tools for Spin Models in Magnetic Systems* (IOP, Bristol, UK, 2021).

[35] Y. Aharonov and D. Bohm, Phys. Rev. **115**, 485 (1959).

[36] A. Eckardt and E. Anisimovas, New J. Phys. **17**, 093039 (2015).

[37] X. G. Wen, F. Wilczek, and A. Zee, Phys. Rev. B **39**, 11413 (1989).

[38] D. J. Thouless, M. Kohmoto, M. P. Nightingale, and M. den Nijs, Phys. Rev. Lett. **49**, 405 (1982).

[39] T. Fukui, Y. Hatsugai, and H. Suzuki, J. Phys. Soc. Jpn. **74**, 1674 (2005).

[40] A. M. León, J. W. González, J. Mejía-López, F. C. de Lima, and E. S. Morell, 2D Mater. **7**, 035008 (2020).

[41] L. D. Landau and E. M. Lifshitz, *Theory of Elasticity*, 3rd ed., Course of Theoretical Physics No. 7 (Elsevier, Amsterdam, 2009).

[42] *Tight-binding Approach to Computational Materials Science: Symposium, December 1–3, 1997, Boston, Massachusetts*, edited by P. E. A. Turchi, A. Gonis, and L. Colombo, Materials Research Society Symposium Proceedings No. 491 (Materials Research Society, Warrendale, PA, 1998).

[43] A. H. Castro Neto and F. Guinea, Phys. Rev. B **75**, 045404 (2007).

[44] J. W. Yoon, Y. G. Kim, I. W. Choi, J. H. Sung, H. W. Lee, S. K. Lee, and C. H. Nam, Optica **8**, 630 (2021).

[45] E. Vinas Boström, M. Claassen, J. McIver, G. Jotzu, A. Rubio, and M. Sentef, SciPost Phys. **9**, 061 (2020).

[46] M. Bukov, M. Kolodrubetz, and A. Polkovnikov, Phys. Rev. Lett. **116**, 125301 (2016).

[47] J. H. Mentink, K. Balzer, and M. Eckstein, Nat. Commun. **6**, 6708 (2015).

[48] M. Claassen, H.-C. Jiang, B. Moritz, and T. P. Devereaux, Nat. Commun. **8**, 1192 (2017).